RESEARCH ARTICLE-PHYSICS

Fabrication and Characterization of Reduced Graphene Oxide/Polyaniline/Poly(Caprolactone) Electrospun Nanofiber

W. Ishwarchand Singh[1] · Sayantan Sinha[1] · Naorem Aruna Devi[1] · Sumitra Nongthombam[1] · Soumyadeep Laha[2] · Bibhu P. Swain[1]

Abstract

Chemically prepared reduced graphene oxide (rGO) and polyaniline (PANI) nanocomposites were synthesized by in situ polymerization monomer of aniline with reduced graphene oxide in acid medium. The rGO/PANI composites were mixed with 10wt% poly(caprolactone) (PCL), and subsequently, the polymeric solution is fabricated into nanofiber by electrospinning method. The XRD data reveal one strong peak at $2\theta = 21.3°$ corresponding to (110) lattice plane for PCL and another two peaks at 24.4° and 30.5° which are indexed at (002) and (322) for rGO and PANI, respectively. The morphology, chemical bonding, microstructure, elemental composition, and optical properties of the rGO/PANI/PCL nanofiber were analyzed by scanning electron microscope, FTIR, Raman, X-ray photoelectron spectroscopy (XPS), UV–visible spectroscopy and photoluminescence spectroscopy, respectively. The Gaussian deconvolution peaks in XPS spectra predict the binding energy of the core orbital in the nanofibers. Moreover, the optical band gap was found to decreases from 4.23 to 4.21 eV with the incorporation of PANI into the electrospun nanofiber.

Keywords Electrospinning · Nanofiber · rGO/PCL · rGO/PANI/PCL · Optical properties

1 Introduction

The electrospun nanofiber has attracted many researchers for its wide application in many fields such as biosensors, drug delivery, biomedical materials, and biomedical applications [1–3]. Electrospinning is a straightforward method used for the fabrication of non-woven fibers continuously with a diameter in the ranges of micro to nanoscales. The electrospun nanofiber possesses many unique properties, such as specific surfaces, excellent mechanical properties, and various designs of surface functionality. The electrospinning of nanofibers using various types of polymers and nanofillers makes it applicable for uses in various field in optoelectronics, catalysis, drug delivery and sensor application [4]. PCL is a bio-resourceful semicrystalline and structurally orthorhombic crystal poly(α-hydroxyester) for its availability at a low

cost and sustaining biodegradability [5]. PCL attracts many applications when reinforced with several conducting materials, ranging from applications in engineering tools to biomedical devices due to a low cellular affinity as a result of poor hydrophilicity and have poor mechanical properties due to its porous nature which limits its application in tissue engineering [6, 7]. Polyaniline (PANI) is reported to have excellent electrical and optical properties with environmentally stable and easy to synthesis. Reduced graphene oxide (rGO) has been extensively adopted as potential nanofillers for improving the physicals and chemical properties of polymeric nanofiber for its unique characteristics such as high conductivity, larger specific surface area, strength, high carrier mobility good optical transparency. Some important progress on PCL/PANI [8–11], PCL/rGO[12–16] and PANI/rGO [17–23] nanocomposites research are investigated extensively in recent years. Farkhondehnia et al. investigated the fabrication of biocompatible PLGA/PCL/PANI nanofibrous scaffolds with electrical excitability [8]. Zhou et al. investigated a highly sensitive ammonia sensor based on spinous core–shell PCL–PANI fibers [9]. Li et al. investigated enhanced adhesion and proliferation of human umbilical vein endothelial cells on conductive PANI-PCL fiber scaffold by electrical stimulation [10]. Rajzer et al.

✉ Bibhu P. Swain
bibhuprasad.swain@gmail.com; bpswain@gmail.com

1 Department of Physics, National Institute of Technology Manipur, Langol, Imphal West, Manipur 795004, India

2 University Science Instrumentation Centre, North Bengal University, Darjeeling, West Bengal 734013, India

investigated conductive PANI patterns on electrospun PCL/ gelatin scaffolds modified with bioactive particles for bone tissue engineering [11]. Miao et al. reported an In situ Study of the Epitaxial Crystallization of PCL/RGO at High Shear Rate [12]. Vijayavenkataraman et al. investigated 3D-Printed PCL/rGO Conductive Scaffolds for Peripheral Nerve Injury Repair [13]. Duan et al. investigated the effect of epitaxial crystallization on the structural evolution of PCL/RGO nanocomposites during stretching by in situ synchrotron radiation [14]. Sanchez et al. investigated evidence of the effect of GO and rGO in PCL membranes on the differentiation and maturation of human neural progenitor cells [15]. Jeong et al. investigated flexible polycaprolactone (PCL) supercapacitor based on reduced graphene oxide (rGO)/single-wall carbon nanotubes (SWNTs) composite electrodes [16]. Han et al. investigated the synthesis of benzenesulfonate PANI/RGO as cathode material for rechargeable lithium-polymer batteries [17]. Sharma et al. investigated enhanced optical and dielectric properties of PANI/rGO nanocomposites for supercapacitor application [18]. Sharma et al. investigated the effect of rGO concentration on the thermal stability of PANI/rGO nanocomposites [19]. Mohamed et al. investigated polyaniline (PANI)/reduced graphene oxide (rGO) composite as a counter electrode for dye solar cells [20]. Zhang et al. investigated the synthesis of PANI/rGO composite as a cathode material for rechargeable lithium-polymer cells [21]. Duan et al. investigated the preparation of rGO/G/PANI ternary nanocomposites as high-performance electrode materials for supercapacitors with spent battery powder as raw material [22]. Mousavi et al. investigated the synergistic effect between redox additive electrolyte and PANI-rGO nanocomposite electrode for high energy and high power supercapacitor [23].

Though many researchers investigated rGO/PCL, PCL/ PANI and rGO/PANI nanocomposites extensively. However, tertiary nanocomposites such as rGO/PCL/PANI nanocomposites were not investigated yet. Therefore, it is paramount important to investigate microstructural, optical properties and compositional study of rGO/PCL/PANI nanocomposites. Hence, the research investigated aimed at following (a) To investigate the morphology and structural properties of rGO/PCL/PANI nanocomposites, (b) To investigate bonding network and optical properties of rGO/PCL/PANI nanocomposites and (c) To investigate the composition and binding network of rGO/PCL/PANI nanocomposites.

2 Experimental

2.1 Materials

PCL (Poly (caprolactone)), $NaNO_3$ (sodium nitrate), hydrazine hydrate, $KMnO_4$ (potassium permanganate), concentrated H_2SO_4 (sulfuric acid), concentrated HCl (hydrochloric acid), H_2O_2 (hydrogen peroxide) (30 vol%), and graphite powder were obtained from Merck Company and Sigma-Aldrich (USA) and all components were used as received without further purification and used as obtained.

2.2 Preparation of GO from Graphite

The GO was synthesized by employing the Hummers' method (modified). Here, graphite powder (5 g) was mixed with $NaNO_3$ (2.5 ml) in a beaker. 120 ml of an acid mixture of H_2SO_4 (98%) and H_3PO_4 (9:1) 120 ml was poured into the mixture of $NaNO_3$ and graphite powder. After stirring the mixture for 15 min under cold conditions, $KMnO_{4+}$ (15 g) was added slowly under constant stirring maintaining the temperature around 15 °C and continuing the stirring for 1 h more. The stirring process was kept on for another 2 h at 40 °C. DI water (250 ml) was poured making the reaction mixture dilute and continue the stirring for 1 h more keeping the temperature at 98 °C. Later, 100 ml of DI is added and continues the stirring at 98 °C. Lastly to reduce the remains of $KMnO_4$, H_2O_2 (30%) (15 ml) was poured into the reaction mixture. After filtration, the pH value of the product is maintained at 7 by washing with DI water. Then, the GO powder is obtained by drying the filtered product inside an oven at 60 °C.

2.3 Synthesis of rGO from GO

The rGO was synthesized by reducing the as-prepared GO. A homogeneous GO suspension was made by dispersing 0.3 g of GO into DI (150) ml water by ultrasonication for about 1 h at room temperature. For reducing the GO, hydrazine hydrate (3 ml) was poured into the GO suspension and kept stirring for 2 h at 80 °C. The color of the GO suspension change from an orange color to black color confirming the reduction processes. After filtration, the reaction product was washed with DI water; later rGO powder was obtained by drying the product overnight in the open air.

2.4 Preparation of rGO/PCL and rGO/PANI/PCL Nanocomposites Solutions

The preparation of rGO/PANI nanocomposite was done by polymerization of aniline with rGO in in situ condition with the help of oxidizing agent of ammonium persulfate in 0.5 M sulfuric acid. 10 wt% PCL solutions were prepared with the mixture of ethanol and chloroform mixing in the ratio of 2:8. Two separated polymeric solutions were prepared for electrospinning in which one contains rGO nanoparticles and 10 wt% PCL solution and the other containing rGO/ PANI nanocomposites with the 10 wt% PCL solution. To get proper dispersion of the mixture, ultrasonicated was done for 2 h.

2.5 Electrospinning

Fabrications of rGO/PCL and rGO/PANI/PCL nanofibers were done by employing the electrospinning method. Firstly, we take a 10 ml glass syringe filled with the polymeric solution. Then, we kept the syringe in a position such that the tip is directing at the middle of the collector mandrel. The collector mandrel is cover thoroughly with aluminum foil and a few glass substrates were mounted on it. Keeping the values of the flow rate of the pump and applied voltage, the electrospinning process is carried out. The mandrel and the needle's tip are kept fixed by 12 cm apart, and the temperature was kept at 30 °C and relative humidity below 40%. The same parameters are fixed to obtain all as nanofibrous structures. At the end of the process, two samples of rGO/PCL and rGO/PANI/PCL nanofiber were obtained. The two samples are kept in the open air for 24 h at room temperature for drying.

3 Characterization

The morphological of the nanofibers obtained were monitor by scanning electron microscope (SEM) (model no: JSM-IT100, JEOL). X-ray diffraction (XRD) pattern of the samples was obtained by using an Advance powder diffractometer, Bruker D8 keeping the scan rate at 0.1% and recorded the data from 10° to 90°. The Raman spectrum was observed by Raman Spectrometer (WITecAlpha300 RS) working with laser sources of 532 nm and fixing the scan rate at 1 cm^{-1}. The X-ray photoelectron spectroscopy (XPS) characterization was done to monitor the elemental composition of the nanofibers by using an X-ray photo spectrometer of model no VG ESCALABMK II with Mg (Kα) at $E = 1.25$ keV for X-ray source. The normalization was succeeded with the help of Au(4f) lines by keeping the pressure of the base chamber at 10^{-10} Torr. FTIR spectrum was obtained to confirm the functional groups present in the nanofibers by using PerkinElmer Spectrum two FTIR Spectrometer having infrared light source keeping and fixing wavenumber ranges from 400 to 4000 cm^{-1}. The optical properties of the rGO/PCL and rGO/PANI/PCL nanofibers were studied by UV–visible spectrometer (Shimadzu UV-1800) which worked with UV–visible light source having the wavelength range from 200 to 4000 nm and keeping 1 nm as the step size. F-7000 Fluorescence Spectrophotometer was used to record the photoluminescence (PL) spectra for the nanofibers. The PL spectra of the nanofibers have been obtained at excitation wavelength 330 nm by using a helium lamp keeping the scan rate = 240 nm/min.

4 Results and Discussion

The morphology of pure PCL, rGO/PCL, and rGO/PANI/PCL nanofibers was analyzed by using SEM. Figure 1 depicts the SEM images of the three nanofibers at the same magnifications, which are deposited uniformly on the glass substrate. The average diameter of rGO/PCL and rGO/PANI/PCL composites nanofibers was found out from the SEM images were by using Image J software. The average diameter of the electrospun nanofibers varied from 154 to 356 nm for pure PCL nanofiber, 93 nm to 251 nm for rGO/PCL, and 139 nm to 620 nm for rGO/PANI/PCL. The rGO is not visible in the composite as the SEM image only gives the idea of surface topology. Figure 1d shows the SEM image of rGO. The SEM images clear indicated various graphene layers. Among the obtained nanofibers, some beads are found to exist which are large in comparison with the nanofibers, resulting due to instabilities in the jet flow of the polymeric solution and accumulation of charge in the jet from the high voltage supply while processing the electrospinning to fabricate the nanofibers.

Figure 2 depicts the XRD spectra for GO and rGO nanocomposites and, rGO/PCL and rGO/PANI/PCL electrospun nanofibers in diffraction angle range $10° \leq 2\theta \leq 50°$. Two intense diffraction peaks were obtained at Bragg angle $2\theta = 21.5°$ and 23.7° corresponding to the (110) and (200) lattice planes for rGO/PCL nanofiber because of orthorhombic crystalline form for polymer PCL [24]. XRD spectra for GO show a sharp peak at 11° corresponding to the (001) plane and for rGO, a broad diffraction peak at around 24° corresponding to (002) diffraction planes are observed. For rGO, the d-spacing which corresponds to the broad peak at (002) is found to be 0.34 nm and for GO, the d-spacing is 0.79 nm corresponds to the (001) plane. The average crystallite size of GO and rGO was estimated to be 1.11 nm and 1.25 nm, respectively. For rGO, the broad peak obtained in the plot indicates the increase in disorder while reducing the GO. For rGO/PANI/PCL electrospun nanofiber reveals one strong peak at $2\theta = 21.3°$ corresponding to (110) lattice plane for PCL and another two peaks at 24.4° and 30.5° which are indexed at (002) and (322) for rGO and PANI, respectively [25].

Figure 3 depicts the FTIR peaks of the pure rGO and PANI nanocomposites along with rGO/PCL and rGO/PANI/PCL nanofibers. In the FTIR spectrum for rGO/PCL nanofiber, a peak at 3443 cm^{-1} is observed which corresponds to stretching of O–H (hydroxyl groups). The confirmation for the presence of PCL spectrum is done by analyzing the sharps bands which includes the stretching –CH$_2$– vibrational peaks observed at 2929 cm^{-1} and the ester bond C=O occurred at 1731 cm^{-1}. The bands at 1238 cm^{-1} and 1168 cm^{-1} are assigned to symmetric

Fig. 1 Scanning electron microscopy images for **a** PCL, **b** rGO/PCL, **c** rGO/PANI/PCL nanofibers and **d** rGO nanoparticle obtained at same magnification
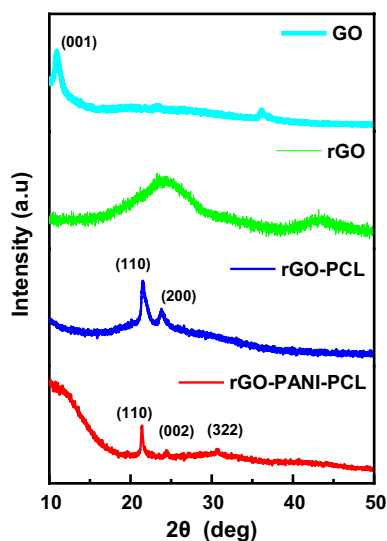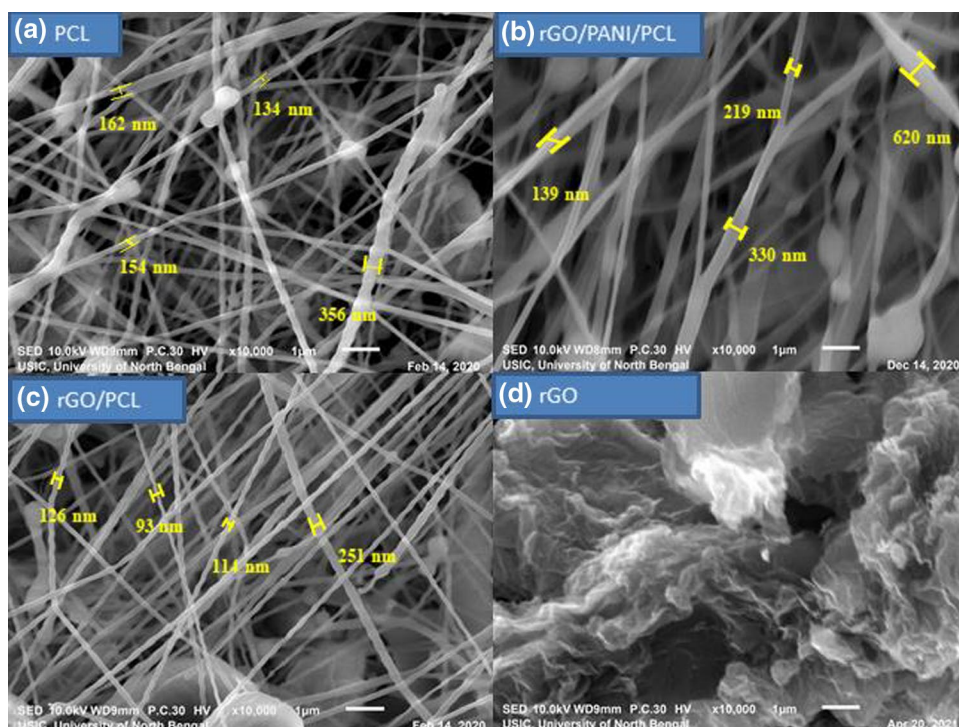

Fig. 2 XRD spectra for GO, rGO, rGO/PCL, and rGO/PANI/PCL

Fig. 3 FTIR spectra for rGO, PANI, rGO/PCL, and rGO/PANI/PCL

C–O–C stretching and the band at 704 cm^{-1} is attributed to backbone C–C rocking which confirms the presence of PCL. The peak at 1238 cm^{-1} assigned to C–O–C bond stretching and the bands at 1037 cm^{-1} and 1238 cm^{-1} have corresponded to the C–C and C–O stretching vibration occurring in the crystalline and amorphous phase of PCL [26–28]. The peaks at 1047 cm^{-1} and 1731 cm^{-1} attributed to C–O–C (epoxy) stretching vibration and stretching vibration of C=O carbonyl indicating the graphite powder being oxidized
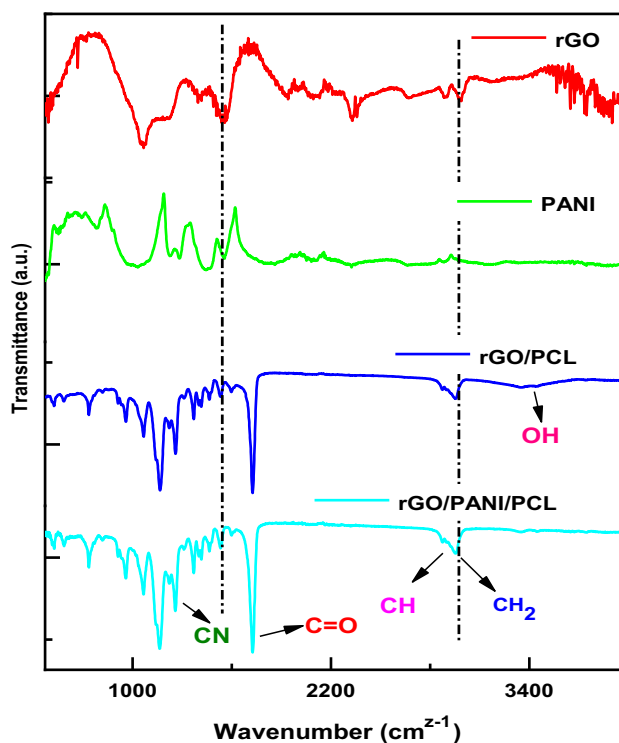
successfully by the Hummers' method. The peak observed at 1450 cm^{-1} assigned to the stretching of water molecules. In the rGO/PANI/PCL nanofiber, peaks obtain at 2957 cm^{-1},

1728 cm^{-1}, 1532 cm^{-1}, 1467 cm^{-1}, 1417 cm^{-1}, 1369 cm^{-1}, 1257 cm^{-1}, 1170 cm^{-1}, and 1064 cm^{-1} are attributed to stretching vibration of C–H bond, C=O ester bond, C=C stretching of a quinoid ring, CH$_2$ bending vibration, due to absorption of a quinoid ring, O–H deformation, C–N stretching, due to stretching of C–O (epoxy) and C–O (alkoxy), respectively [29, 30].

Figure 4a depicts the Raman peaks for pure rGO nanocomposite and rGO/PCL and rGO/PANI/PCL nanofibers. Four characteristic peaks for GO and rGO are observed at 1323 cm^{-1}, 1598 cm^{-1}, 2604 cm^{-1}, and 2810 cm^{-1} corresponding to the D band, G band, 2D, and D + G bands, respectively. In the rGO spectrum, the D band is attributed

to the structural defects or presence of sp^3 hybridization carbon atoms and the G band is related to the energy of the bonds or sp^2 hybridization graphitic domains. Moreover, the 2D band is associated with the graphene monolayer's second-order vibrations. In the rGO network, the sp^2 carbon is attached with oxygen; however, in PCL/rGO, the sp^2 is attached with higher electronegative atoms such as nitrogen and carbon. Therefore, Raman shift changes. In the composite sample, the percentage composition of rGO is only 5%; therefore, the D band and G band appeared to be very weak. The characteristic bands of the PCL polymer are present in the rGO/PCL and rGO/PANI/PCL nanofibers. The weak absorption bands at 1439 cm^{-1} and 1729 cm^{-1} are assigned

Fig. 4 **a** Broad Raman spectra, **b** deconvolution spectra for the 1st order peaks, **c** deconvolution plots for second-order Raman spectra for GO, rGO nanocomposites, and rGO/PCL and rGO/PANI/PCL nanofibers
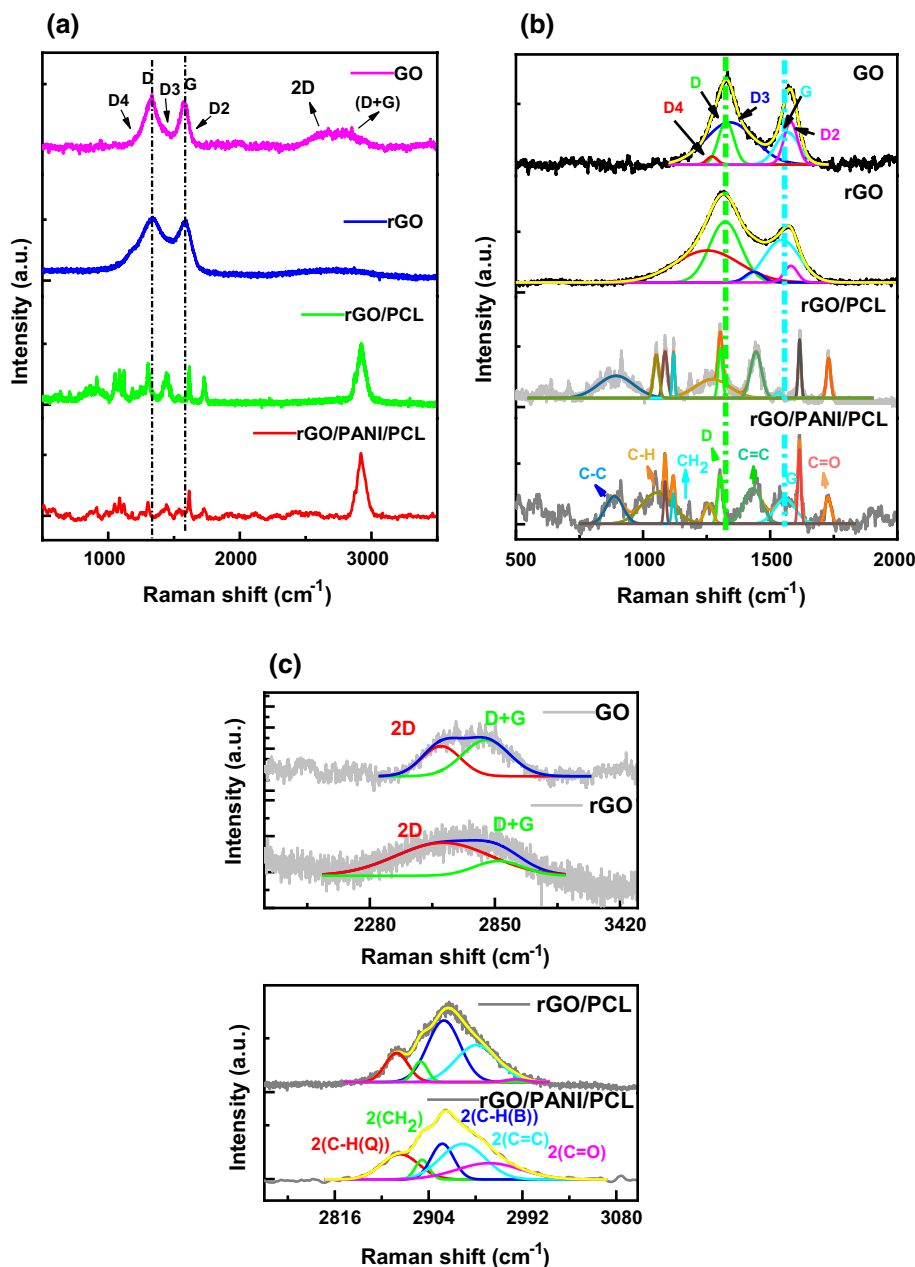
to the ester group CH$_2$ and C=O vibrations, respectively [31]. Another two peaks at 2922 cm^{-1} and 1729 cm^{-1} in the spectrum of pure rGO/PCL and rGO/PANI/PCL nanofibers correspond to the stretching vibrations of C–H and C=O bonds [32]. The skeletal stretching vibrations of C–C peaks were observed at 1060 cm^{-1}, out-of-plane wagging vibration of C–H at 1284 cm^{-1}, and the bending vibrations of C–H at 1433 cm^{-1}. Also, the peaks observed at 887 cm^{-1} were attributed to stretching vibrations C–C. At 2934 cm^{-1} and 1729 cm^{-1}, two peaks are obtained the corresponding bending and stretching vibration of –CH$_2$ and –C=O bonds of neat PCL. At 1621 cm^{-1}, C=C bond vibration is observed for GO. However, the representative bands for rGO, i.e., D and G are appearing in both the rGO/PCL and rGO/PANI/PCL nanofibers as observed in the deconvoluted plots, and also the representative peaks for PCL polymers are appearing in the spectra of the two composite nanofibers. These results suggest the possibility of interactions between rGO nanofillers and the PCL polymer matrix [33, 34].

Figure 4b exhibits the deconvoluted plot for first-order Raman peaks observed in GO, rGO, rGO/PCL nanofiber, and rGO/PANI/PCL nanofiber. The five Gaussian peaks observed in the deconvoluted GO and rGO Raman spectra correspond to the five bands D1, D, D2, D3, and G. To analyze the disorder present in the structure of the graphite, the I_D/I_G ratios are calculated. The I_D/I_G ratio was found to be 1.12 and 0.78 for GO and rGO, respectively, suggesting a lesser degree of defect in rGO than GO. The deconvoluted Gaussian peaks obtained at 887 cm^{-1}, 1060 cm^{-1}, 1284 cm^{-1}, 1302 cm^{-1}, 1433 cm^{-1}, 1567 cm^{-1}, 1615 cm^{-1}, and 1729 cm^{-1} are attributed to the different functional groups for the rGO, PANI, and PCL composites as discussed above [33–35].

Figure 4c illustrates the deconvoluted second-order plot for the GO and rGO nanocomposites and, rGO/PCL and rGO/PANI/PCL nanofibers. The two bands obtained in the range 2400–3000 cm^{-1} in the deconvoluted second-order Raman spectra for both GO and rGO are attributed to the 2D band and the G + D band. The intensity ratio of 2D and G bands is associated with the numbers of the graphene layer, and a higher value suggests larger numbers of graphene layers present in the graphite structure. On the other hand, the I_{2D}/I_G ratio of the rGO is 0.37, suggesting the graphene structure is maintained. The I_{2D}/I_G of the GO was found to be 1.13 which means a turbostratic structure. The Gaussian peaks that observed in both the deconvoluted Raman spectra of rGO/PCL and rGO/PANI/PCL nanofiber are attributed to 2(C–H(Q)), 2(CH$_2$), 2(C–H(B)), and 2(C=O) bonds, respectively [36, 37].

Figure 5a illustrates the ultraviolet–visible spectroscopy absorption peaks of the rGO/PCL and rGO/PANI/PCL nanocomposites. UV–visible spectroscopy gives a peak shouldering at 278 nm to 289 nm attributing to the n–π* transition

in the C–O bond. The bandgap was determined by plotting the data of optical absorbance along with the concerning energy [38–40]. The optical bandgap was found out from Tauc's plot, i.e., $(\alpha h\nu)^2$ versus $h\nu$ plot. The optical bandgap was obtained by extrapolating the linear portion of the curves to intercept the x-axis where the y-axis is zero, i.e., zero absorption as $h\nu$-axis at $\alpha = 0$ as shown in Fig. 5b. The Tauc's bandgap of rGO/PANI/PCL and rGO/PCL are 4.21 and 4.23 eV, respectively. The optical bandgap of rGO/PCL slightly decreases with the incorporation of PANI in rGO/PCL/PANI nanocomposites. The decreasing or increasing of optical bandgap in an alloying can be explained by Végard's relationship,
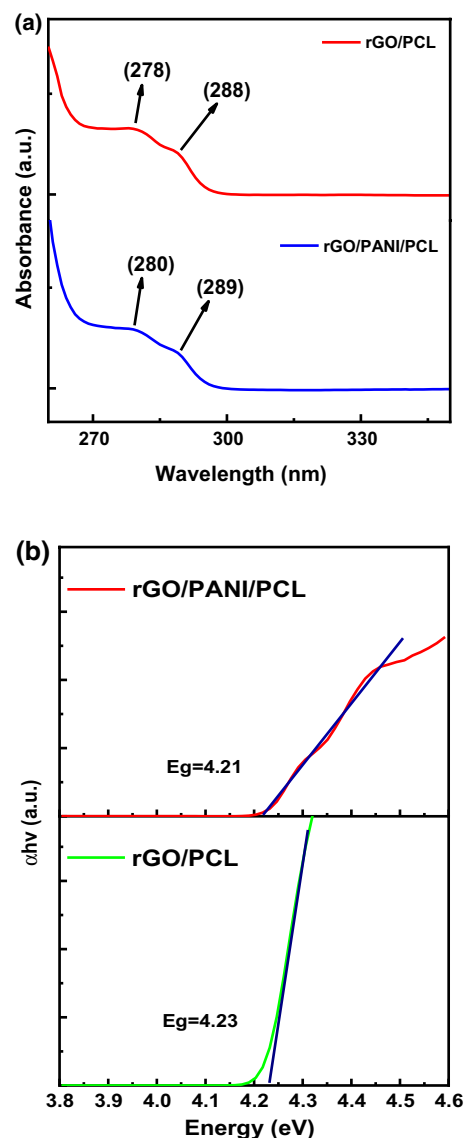

Fig. 5 a UV–visible absorption spectra, **b** Tauc's plot for rGO/PCL and rGO/PANI/PCL nanocomposites

$$E_g^{AB} = xE_g^A + (1-x)E_g^B - bx(1-x) \qquad (1)$$

where E_g^A, E_g^B and E_g^{AB} are bandgap of A, B and its alloys, respectively, where b is the bowing factor due to alloying. x and $(1-x)$ are the fractional composition of A and B semiconductors. The optical band gap of PANI is 2.4 eV, therefore, for $x = 0.1$ for PANI content and estimated bowing factor, $b = 1.811$.[41].

The elemental composition of the rGO/PCL and rGO/PANI/PCL nanofibers surface was studied by XPS analysis. Figure 6a displays the broad scan XPS plot of the rGO/PCL nanofibers having two elements: O (1s) and C (1s) at 527 eV and 284 eV, respectively, and for rGO/PANI/PCL nanofibers three elements are founds, O (1s), N (1s), and C (1s) at 527 eV, 399 eV and 284 eV, respectively. As XPS is surface analysis, the soft X-ray can penetrate only up to 15 nm, and that element that appeared at the less at.% difficult to get at the broad spectrum. Therefore, the N signal is low.

Figure 6b illustrates the deconvolution of the XPS plot for C (1s) core orbital for rGO/PCL and rGO/PANI/PCL nanofibers. In the two samples for PCL-rGO and rGO/PANI/PCL nanofibers, four deconvoluted gaussian peaks were observed for C(1s) core orbital for each sample. The four peaks being centered at approximately 290.4 eV, 287.13 eV, 284.5 eV, and 282.3 eV attributed to O–C–O/C=O, C–O, C=C, and C–C bonds, respectively. For PCL-rGO nanofiber, O–C–O/C=O, C–O, C=C, and C–C appeared at the binding energies 288.94 eV, 286.53 eV, 285.02 eV, and 282.33 eV, respectively. The areal ratios of the bonds O–C–O/C=O, C–O, C–C, and concerning to C=C bond are 0.659, 0.134, and 0.076, respectively, for the PCL-rGO nanofiber. Similarly, for rGO/PANI/PCL nanofiber, the deconvoluted gaussian peaks at 288.80 eV, 287.12 eV, 286.06 eV, and 284.70 eV are attributed to O–C–O/C=O, C–N, C–O, and C=C bonds, respectively. In rGO/PANI/PCL nanofiber, we didn't recognize the C–C bond, but we find in rGO/PCL nanofiber, which indicate that carbon has been attached with a higher electronegative element such as nitrogen and form bond like C–N bond. The areal ratios of the bonds O–C–O/C=O, C–N, C–O,

Fig. 6 **a** XPS survey scan, **b** deconvoluted plot for C (1s) core orbital, **c** deconvoluted plot for O (1s) core orbital for pure rGO/PCL and rGO/PANI/PCL nanofibers, and **d** deconvoluted plot for N (1s) core orbital for rGO/PANI/PCL nanofibers
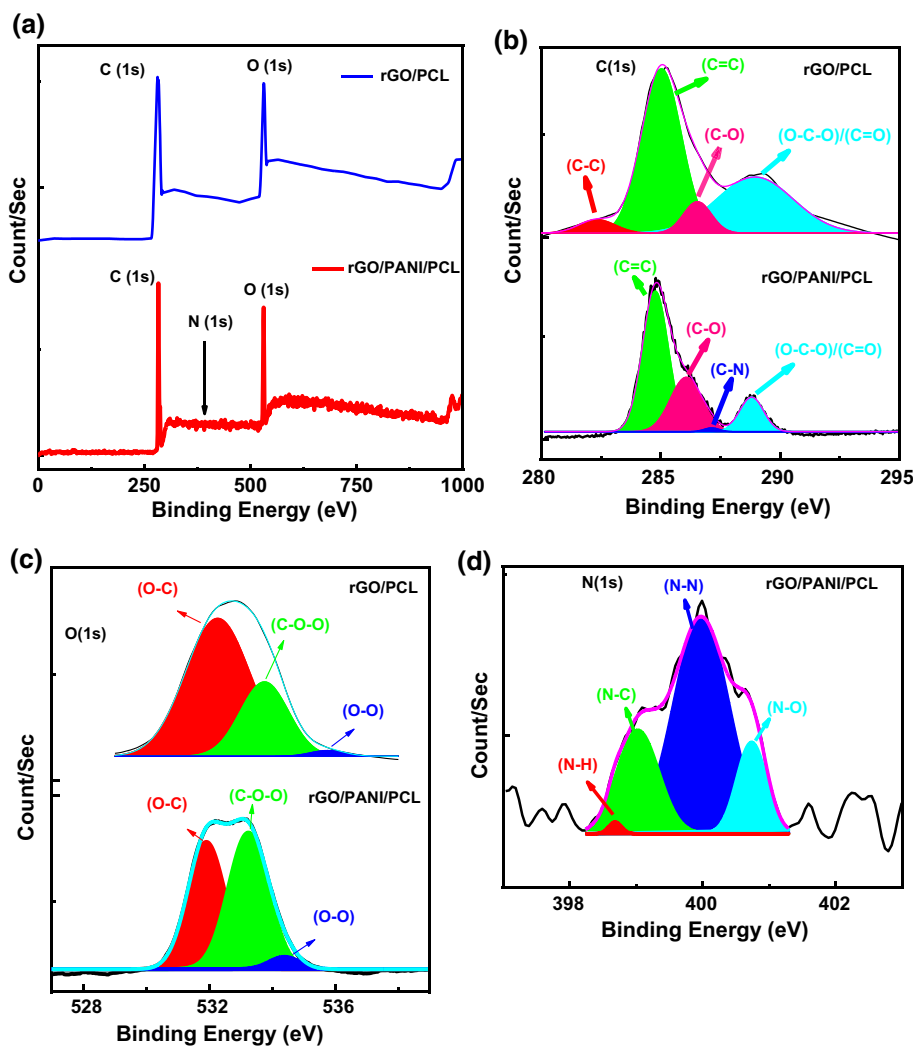
and concerning to C=C bond are 0.226, 0.015, and 0.473, respectively, for the rGO/PANI/PCL nanofiber [42].

Figure 6c illustrates the deconvolution of XPS spectra for O (1s) core orbital for pure rGO/PCL and rGO/PANI/PCL nanofibers. In the two samples for rGO/PCL and rGO/PANI/PCL nanofibers, three deconvoluted gaussian peaks were observed for O (1s) core orbital for each sample. The three peaks being centered at approximately 533.350 eV, 532.18 eV, and 531.28 eV attributed to O–O, C–O–C, and O–C, bonds, respectively. For rGO/PCL nanofiber, O–O, C–O–C, and O–C bonds appeared at the binding energies 535.750 eV, 533.747 eV, and 532.261 eV, respectively. The areal ratios of the bonds O–C and C–O–C concerning O–O bond are 44.366 and 17.88, respectively, for the rGO/PCL nanofiber. Similarly, for rGO/PANI/PCL nanofiber, the deconvoluted gaussian peaks at 531.89 eV, 533.23 eV, and 534.38 eV are attributed to O–C, C–O–C, and O–O bonds, respectively. The areal ratios of the O–C and C–O–C bonds concerning O–O bond are 12.61 and 14.43, respectively, for the rGO/PANI/PCL nanofiber [42–44].

Figure 6d illustrates the deconvoluted XPS peaks for N (1s) core orbital for rGO/PANI/PCL nanofibers. In the rGO/PANI/PCL nanofibers, four deconvoluted gaussian peaks were observed for N (1s) core orbital for each sample. The four peaks being centered at approximately 400.73 eV, 399.97 eV, 399.024 eV, and 398.68 eV attributed to N=O, N–O, N–N, and N–C bonds, respectively. The areal ratios of the N–C, N–O and N=O bonds concerning to N–N bond are 0.035, 32.856, and 0.624, respectively, for the rGO/PANI/PCL nanofiber.

Figure 7 shows the photoluminescence (PL) emission spectra of rGO/PCL and rGO/PANI/PCL. The carrier mobility of the rGO has a higher value resulting in the reduction of the recombination rate in the two nanofibers sample. The two nanofibers, namely rGO/PCL and rGO/PANI/PCL showed a broad PL emission peak from 400 to 500 nm and one less intense peak centered at 729 nm with excitation at 358 nm. The PL emission peaks are appeared mainly due to rGO contain in the nanofibers. After the reduction of GO, the number of disorder-induced states that appeared in the π–π* gap of the rGO decreases, thus increasing the amount of small size sp^2 clusters in the rGO which led to show blue luminescence. Interestingly, the peak intensity was increased of the two nanofibers in the order of rGO/PANI/PCL than rGO/PCL which confirmed that the charged carriers' recombination was very high in rGO/PANI/PCL which may be due to the incorporation of PANI [43].

5 Conclusion

In this study, we prepared rGO and PANI nanocomposites by incorporating rGO nanoparticles during in situ polymerizations of aniline monomer in acidic conditions.
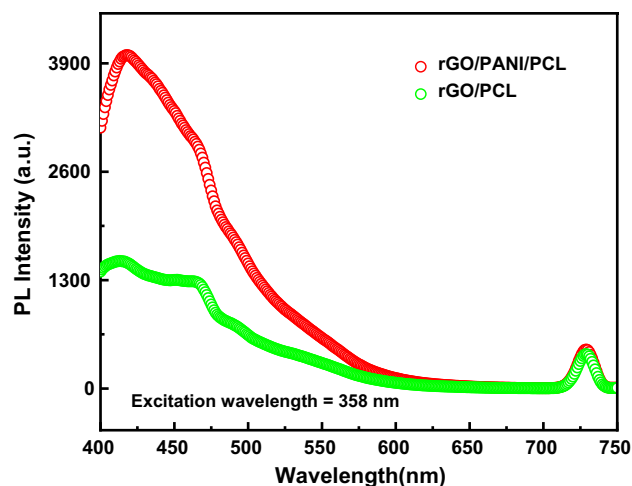

Fig. 7 Photoluminescence emission spectra for rGO/PCL and rGO/PANI/PCL nanocomposites

We fabricated rGO/PANI/PCL and rGO/PCL nanofibers via the electrospinning method for comparative studies. The SEM analysis of the nanofibers gives the averages diameter of the nanofiber which is found to be 93 nm to 620 nm. The XRD pattern of the rGO/PANI/PCL electrospun nanofiber reveals one strong peak at $2\theta = 21.3°$ corresponding to (110) lattice plane for PCL and another two peaks at 24.4° and 30.5° which are indexed at (002) and (322) for rGO and PANI, respectively. Chemical bonding analysis was done by FTIR and Raman spectroscopy. UV–visible spectroscopy analysis showed a peak shouldering at 278 nm to 289 nm attributed to the n–π* transition. Moreover, the optical band gap was found to decreases from 4.23 to 4.21 eV with the incorporation of PANI into the electrospun nanofiber. In the XPS study, two sharp peaks were obtained at 527 eV and 284 eV corresponds to O(1s) and C(1s) respectively, and one small peak at 399 eV corresponding to N (1s).

Declarations

Conflict of interest The authors declare that there is no conflict of interest that is relevant to the content of this article.

References

1. Sun, H.; Mei, L.; Song, C.; Cui, X.; Wang, P.: The in vivo degradation, absorption, and excretion of PCL-based implant. Biomaterials **27**, 1735–1740 (2006)

2. Chandra, R.; Rustgi, R.: Biodegradable polymers. Prog. Polym. Sci. **23**, 1273–1335 (1998)

3. Lu, W.; Sun, J.; Jiang, X.: Recent advances in electrospinning technology and biomedical applications of electrospun fibers. J. Mater. Chem. B **2**, 2369–2380 (2014)

4. Lekakou, C.; Wilson, P.; Craggs, D.; Chau, Y.C, Salifu A.A, Chen Y.L, Watts J.F.: Edinburgh ICCM17 Proceedings of 17th International Conference on Composite Materials (2009).

5. Basavaraja, C.; Kim, D.G.; Kim, W.J.; Kim, J.H.; Huh, D.S.: Morphology and charge transport properties of chemically synthesized polyaniline-poly(ε-caprolactone) polymer films. Bull. Korean Chem. Soc. **32**, 3927 (2011)

6. Kim, H.; Abdala, A.A.; Macosko, C.W.: Graphene/polymer nanocomposites. Macromolecules **43**, 6515–6530 (2010)

7. Wan, C.; Chen, B.: Poly (ε-caprolactone)/graphene oxide biocomposites: mechanical properties and bioactivity. Biomed. Mater. **6**, 055010 (2011)

8. Farkhondehnia, H.; Amani Tehran, M.; Zamani, F.: Fabrication of biocompatible PLGA/PCL/PANI nanofibrous scaffolds with electrical excitability. Fibers Polym. **19**(9), 1813–1819 (2018). https://doi.org/10.1007/s12221-018-8265-1

9. Zhou, W.; Guo, Y.; Zhang, H.; Su, Y.; Liu, M.; Dong, B.: A highly sensitive ammonia sensor based on spinous core–shell PCL–PANI fibers. J. Mater. Sci. **52**(11), 6554–6566 (2017). https://doi.org/10.1007/s10853-017-0890-3

10. Li, Y.; Li, X.; Zhao, R.; Wang, C.; Qiu, F.; Sun, B.; Ji, H.; Qiu, J.; Wang, C.: Enhanced adhesion and proliferation of human umbilical vein endothelial cells on conductive PANI-PCL fiber scaffold by electrical stimulation. Mater. Sci. Eng. C **72**, 106–112 (2017). https://doi.org/10.1016/j.msec.2016.11.052

11. Rajzer, I.; Rom, M.; Menaszek, E.; Pasierb, P.: Conductive PANI patterns on electrospun PCL/gelatin scaffolds modified with bioactive particles for bone tissue engineering. Mater. Lett. **138**, 60–63 (2015). https://doi.org/10.1016/j.matlet.2014.09.077

12. Miao, W.; Wu, F.; Wang, Y.; Wang, Z.: In-situ study of the epitaxial crystallization of PCL/RGO at high shear rate by in situ SAXS/WAXD methods. ACS Omega **5**(49), 31535–31542 (2020). https://doi.org/10.7503/cjcu20200493

13. Vijayavenkataraman, S.; Thaharah, S.; Zhang, S.; Lu, W.F.; Fuh, J.Y.H.: 3D-printed PCL/rGO conductive scaffolds for peripheral nerve injury repair. Artif. Organs **43**(5), 515–523 (2019). https://doi.org/10.1111/aor.13360

14. Duan, T.; Xu, H.; Tang, Y.; Jin, J.; Wang, Z.: Effect of epitaxial crystallization on the structural evolution of PCL/RGO nanocomposites during stretching by in-situ synchrotron radiation. Polymer **159**, 106–115 (2018). https://doi.org/10.1016/j.polymer.2018.11.020

15. González, S.S.; Diban, N.; Bianchi, F.; Ye, H.; Urtiaga, A.: Evidences of the effect of GO and rGO in PCL membranes on the differentiation and maturation of human neural progenitor cells. Macromol. Biosci. **18**(11), 1800195 (2018). https://doi.org/10.1002/mabi.201800195

16. Jeong, H.T.; Kim, Y.R.; Kim, B.C.: Flexible polycaprolactone (PCL) supercapacitor based on reduced graphene oxide (rGO)/single-wall carbon nanotubes (SWNTs) composite electrodes. J. Alloys Compd. **727**, 721–727 (2017). https://doi.org/10.1016/j.jallcom.2017.07.335

17. Han, T.; Han, J.-J.; Ma, H.; Zhang, N.; Sun, D.-D.: Synthesis of benzenesulfonated PANI/RGO as cathode material for rechargeable lithium-polymer batteries. Ionics **25**(10), 4739–4749 (2019). https://doi.org/10.1007/s11581-019-03040-2

18. Sharma, A.K.; Jain, P.K.; Vyas, R.; Mathur, V.; Jain, V.K.: Enhanced optical and dielectric properties of PANI/rGO nanocomposites for supercapacitor application. J. Nano-Electron. Phys. **11**(5), 05026 (2019). https://doi.org/10.21272/jnep.11(5).05026

19. Sharma, A.K.; Jain, P.K.; Vyas, R.; Mathur, V.; Jain, V.K.: Effect of rGO concentration on the thermal stability of PANI/rGO nanocomposites. J. Nano-Electron. Phys. **11**(5), 05042 (2019). https://doi.org/10.21272/jnep.11(5).05042

20. Mohamed, N.M.; Shahid, M.U.; Mahinder Singh, B.S.; Joseph, E.; Mohamed Saheed, M.S.; Yar, A.; Bashiri, R.: Polyaniline (PANI)/reduced graphene oxide (rGO) composite as a counter electrode for dye solar cells. IOP Conf. Ser.: J. Phys. **1123**(1), 012012 (2018). https://doi.org/10.1088/1742-6596/1123/1/012012

21. Zhang, R.-T.; Han, J.-J.; Liu, P.; Bao, C.-Y.; Cheng, J.-N.: Synthesis of PANI/rGO composite as a cathode material for rechargeable lithium-polymer cells. Ionics **24**(11), 3367–3373 (2018). https://doi.org/10.1007/s11581-018-2525-3

22. Duan, X.; Deng, J.; Wang, X.; Liu, P.: Preparation of rGO/G/PANI ternary nanocomposites as high-performance electrode materials for supercapacitors with spent battery powder as raw material. Mater. Des. **129**, 135–142 (2017). https://doi.org/10.1016/j.matdes.2017.05.031

23. Mousavi, M.F.; Hashemi, M.; Rahmanifar, M.S.; Noori, A.: Synergistic effect between redox additive electrolyte and PANI-rGO nanocomposite electrode for high energy and high power supercapacitor. Electrochim. Acta **228**, 290–298 (2017). https://doi.org/10.1016/j.electacta.2017.01.027

24. Wang, K.; Li, W.; Gao, C.: Poly (caprolactone) functionalized carbon nanofibers by surface-initiated ring-opening polymerization. J. Appl. Polym. Sci. **105**, 629–640 (2007). https://doi.org/10.1002/app.26285

25. Gao, W.; Alemany, L.B.; Ci, L.; Ajayan, P.M.: New insights into the structure and reduction of graphite oxide. Nat. Chem. **1**, 403 (2009). https://doi.org/10.1038/nchem.281

26. Bhadra, S.; Khastgir, D.: Determination of crystal structure of polyaniline and substituted polyanilines through powder X-ray diffraction analysis. Polym. Testing **27**, 851–857 (2008). https://doi.org/10.1016/j.polymertesting.2008.07.002

27. Ramezanzadeh, B.; Niroumandrad, A.; Ahmadi, M.; Mahdavian, M.H.; Mohamadzadeh, M.: Enhancement of barrier and corrosion protection performance of an epoxy coating through wet transfer of amino functionalized graphene oxide. Corros. Sci. **103**, 283–304 (2016). https://doi.org/10.1016/j.corsci.2015.11.033

28. Bhujel, R.; Swain, B.P.: Investigation of cyclic voltammetry and impedance spectroscopy of thermally exfoliated biomass synthesized nickel decorated graphene. J. Phys. Chem. Solids **130**, 242–249 (2019). https://doi.org/10.1016/j.jpcs.2019.02.023

29. Swain, B.P.: Influence of process pressure on HW-CVD deposited a-SiC: H films. Surf. Coat. Technol. **201**(3–4), 1132–1137 (2006). https://doi.org/10.1016/j.surfcoat.2006.01.059

30. Bhujel, R.; Rai, S.; Baruah, K.; Deka, U.; Biswas, J.; Swain, B.P.: Capacitive and sensing responses of biomass-derived silver decorated graphene. Scientific Rep. **9**, 1–14 (2019). https://doi.org/10.1038/s41598-019-56178-4

31. Swain, B.P.: The analysis of the carbon bonding environment in HWCVD deposited a-SiC: H films by XPS and Raman spectroscopy Surf. Coat. Technol. **201**, 1589–1593 (2006). https://doi.org/10.1016/j.surfcoat.2006.02.029

32. Rai, S.; Bhujel, R.; Biswas, J.; Swain, B.P.: Effect of electrolyte on the supercapacitive behaviour of copper oxide/reduced graphene oxide nanocomposite. Ceram. Int. **45**, 14136–14145 (2019). https://doi.org/10.1016/j.ceramint.2019.04.114

33. Nongthombam, S.; Devi, N.A.; Sinha, S.; Bhujel, R.; Rai, S.; Ishwarchand, W.; Laha, S.; Swain, B.P.: Reduced graphene oxide/

Springer

gallium nitride nanocomposites for supercapacitor applications. J. Phys. Chem. Solids **141**, 109406 (2020). https://doi.org/10.1016/j.jpcs.2020.109406

34. Swain, B.P.; Swain, B.S.; Hwang, N.M.: Investigation of local order of a-SiN: H films deposited by hot wire chemical vapour deposition (HWCVD). Appl. Surf. Sci. **255**(5), 2557–2560 (2008). https://doi.org/10.1016/j.apsusc.2008.07.151

35. Bhujel, R.; Rai, S.; Deka, U.; Swain, B.P.: Electroch emical, bonding network, and electrical properties of reduced graphene oxide-Fe$_2$O$_3$ nanocomposite for supercapacitor electrodes applications. J. Alloys Compd. **792**, 250–259 (2019). https://doi.org/10.1016/j.jallcom.2019.04.004

36. Swain, B.P.; Dusane, R.O.: Effect of filament temperature on HWCVD deposited a-SiC: H. Mater. Lett. **60**(24), 2915–2919 (2006). https://doi.org/10.1016/j.matlet.2005.10.050

37. Swain, B.S.; Swain, B.P.; Hwang, N.M.: Chemical surface passivation of silicon nanowires grown by APCVD. Curr. Appl. Phys. **10**(3), S439–S442 (2010). https://doi.org/10.1016/j.cap.2009.12.029

38. Devi, N.A.; Nongthombam, S.; Sinha, S.; Bhujel, R.; Rai, S.; Singh, W.I.; Dasgupta, P.; Swain, B.P.: Investigation of chemical bonding and supercapacitivity properties of Fe$_3$O$_4$-rGO nanocomposites for supercapacitor applications. Diam. Relat. Mater. **104**, 107756 (2020). https://doi.org/10.1016/j.diamond.2020.107756

39. Sinha, S.; Devi, N.A.; Nongthombam, S.; Bhujel, R.; Rai, S.; Sarkar, G.; Swain, B.P.: Investigation of optical, electrical and electrochemical properties of polyaniline/rGO/Ag$_2$O nanocomposite. Diam Relat Mater. **107**, 107885 (2020). https://doi.org/10.1016/j.diamond.2020.107885

40. Rai, S.; Bhujel, R.; Biswas, J.; Swain, B.P.: Effect of electrolyte on the supercapacitive behaviour of copper oxide/reduced graphene oxide nanocomposite. Ceram. Int. **45**(11), 14136–14145 (2019). https://doi.org/10.1016/j.ceramint.2019.04.114

41. Singh, J.: Physics of Semiconductors and Their Heterostructures, Chapter 6, p. 180. McGraw-Hill.

42. Swain, B.P.; Hwang, N.M.: Effect of negative substrate bias on HWCVD deposited nanocrystalline silicon (nc-Si) films. Solid State Sci. **11**(2), 467–471 (2012). https://doi.org/10.1016/j.solidstatesciences.2008.08.004

43. Swain, B.S.; Lee, S.S.; Lee, S.H.; Swain, B.P.; Hwang, N.M.: Effect of H$_2$ ambient annealing on silicon nanowires prepared by atmospheric pressure chemical vapor deposition. Chem. Phys. Lett. **494**(4–6), 269–273 (2012). https://doi.org/10.1016/j.cplett.2010.06.028

44. Susheel, K.S.; Arvind, K.V.; Shukla, R.K.: Synthesis and optical studies of pure polyaniline film. Int. J. Curr. Microbiol. Appl. Sci. **3**, 512–517 (2014)